(IJRST) 2018, Vol. No. 8, Issue No. II, Apr-Jun **e-ISSN: 2249-0604, p-ISSN: 2454-180X**

DURABILITY OF RECYCLED LIME-FLYASH TREATED AGGREGATES AS PAVEMENT BASE MATERIALS ----- CHINESE EXPERIENCE

***Guoqiang Zhao, **Zheng Sun, ***Donglan Su, ****Junan Shen**

**Senior Engineer, CCDI (Suzhou) GROUP, Jiangsu 215011, China*

***Graduate student, Department of Civil Engineering*

Suzhou University of Since and Technology, Suzhou, Jiangsu, 215001, China

****Lecture, Department of Civil Engineering*

Suzhou University of Since and Technology, Suzhou, Jiangsu, 215001, China

*****Ph.D. Professor, Department of Civil Engineering*

Suzhou University of Since and Technology, Suzhou, Jiangsu, 215001, China

Department of Civil Engineering and Construction

Georgia Southern University, Statesboro, GA, USA

ABSTRACT

This study investigated the long-term properties of recycled lime-flyash treated aggregates (RTA) as pavement base and subbase layers. First, the both the physical and chemical properties of the waste lime-flyash treated aggregate (WTA) materials were tested. Then, RTA were designed according to the specifications and further examined for its long-term durability properties including shrinkage, freeze-thaw, fatigue and permeability. The RTA investigated were actually cement-stabilized RTA, a stabilized blend of 70% WTA and 30% virgin aggregates for base layer, and a stabilized 100% WTA for subbase layer, respectively. Test results were as follows: 1) WTA particle surfaces were becoming rougher as the size of the particles decreased, which was closely related to the degree of shrinkages of the RTA. 2) Both the value of moisture shrinkage and the weight of water loss of RTA increased as the curing time of RTA increased, indicating the contribution of the weight loss to the shrinkage of the RTA. 3) The total thermal shrinkage increased as temperature decreased although its rate of increase decreased for every temperature increment. 4) Overall, the fatigue life of RTA was short, indicting its structure was closer to that of suspension dense type.

Keywords: *lime-flyash stabilized; long-term performance; cement-stabilized; moisture and thermal shrinkage; fatigue; freeze-thaw*

INTRODUCTION

Lime-flyash stabilized aggregates have been widely used as either a road base or a subbase layer materials in China since early 1970. Some of these roads built with the lime-flyash stabilized aggregates needs to maintain or to reconstruct, resulting in a large number of waste lime-flyash stabilized aggregates (WTA) (1, 2, 3). The huge amount of WTA will take up a landfill, consequently, pollute the environment. How to deal with these WTA becomes a problem faced to road engineers (4, 5). The use of WTA can reduce the cost of road construction, and the pollution on environment. Studies showed that cost reduction was observed by stabilizing unsuitable roadway materials with high carbon flyash (9, 10). WTA is better than these unsuitable roadway materials in engineering properties. It will be expected more economical when WTA is recycled effectively (11). WTA proved to contain some clay and flyash(12), which can effectively improve the frost resistance of the stabilized WTA (13).

Researches available on disposal of the WTA showed that the surface of WTA was covered with a layer of lime-flyash (stabilizer) mortar. The mortar appears mostly rough surfaces with a high water absorption, and makes it difficult in compacting recycled lime-fly ash treated aggregates with a stabilizer (RTA) as a base and sub-base layer materials. On the other hand, the mortar may contain some active chemical compounds that will benefit to the strength of the RTA. The presence of surface mortar on the waste aggregates will negatively affect the performance of the RTA (6, 7, 8).Removal of the surface mortar will not only greatly increase the cost, but also cause second pollution to the environment. The properties of the RTA have uncertainty, depending on the properties of the WTA, and then concerned for their long term performance. The properties of RTA were affected by the aggregate size and gradation. The compacting condition of aggregate was the main reason for the performance of RTA. Under the same compaction conditions, the coarse aggregate with continuous gradation can form a better a skeleton structure (14, 15, 16).

When used for road base or subbase layer materials, both the thermal and moisture shrinkages of the RTA come up as a difficult problem.Studies have shown that each decrease in temperature will lead to a temperature-caused shrinkage. Even if the shrinkage does not produce a direct crack to the material, the material will be subject to a stress causing fatigue (17, 18). The key factors to make RTA materials by cement as a road base lies in the long-term performance such as the thermal crack resistance. Several studies proved that the cement dose, and the gradation of aggregates were the two crucial factors to the shrinkage cracks (19, 20). A cement dose of 3 to 4% will generate a minimum dry shrinkage strain and coefficient that increased linearly with its dosage. The denser the RTA and the coarser the gradation, the smaller the dry shrinkage strain of RTA.

The objective of this study was to investigate the long-term durability of using WTA

(IJRST) 2018, Vol. No. 8, Issue No. II, Apr-Jun **e-ISSN: 2249-0604, p-ISSN: 2454-180X**

stabilized by cement as both a road base and a sub-base material, and how the performance of the RTA was affected by the physical and chemical properties of the WTA. To this end, cement-stabilized RTAs were first designed meeting with the specifications of base and subbase. Second, long-term properties of the RTAs were evaluated in terms of a series of laboratory experiment tests including thermal and moisture shrinkage, freeze-thaw, and fatigue and permeability. The physical and mechanical properties of WTA (density and water absorption, LA abrasion, crush-resistance) were explore their effects on the durability of the RTA materials.

MATERIALS AND TEST METHODS

MATERIALS

Waste lime-flyash stabilized aggregates (WTA) used for the study came from Route 328, Taicang, Jiangsu, China. Figure 1 presented the outlook of the WTA in different three different size: coarse (>4.75mm), fine (4.75~0.075mm) and filler (<0.075mm). The WTA was divided into the three size ranges to design a combined gradation for RTA meeting with the specifications as base materials.

a) >4.75mm b) 4.75~0.075mm c) <0.075mm

Figure 1 the outlook of the WTA in different size range

Gradation

In order to accurately measure the gradation of the WTA, WTAs were sieved by following a wet sieving method (WTA contains more fine aggregate, the wet sieving method will be more accurate.), and virgin aggregates by following a dry sieving method. Virgin aggregates of two size range, i.e., NO.1 (31.5 ~ 19 mm) and NO.2 (19 ~ 9.5 mm), were used considering the requirement of the combined gradation. The grading results of both WTA and the virgin aggregates were shown in Table 1.

A blend of 70% of WTA, 20% NO.1 (virgin aggregates) and 10% NO.2 (virgin aggregates) was finally designed, as for base materials, meeting with the specifications of JTG/E51-2009(21). A

(IJRST) 2018, Vol. No. 8, Issue No. II, Apr-Jun **e-ISSN: 2249-0604, p-ISSN: 2454-180X**

100% of WTA, used for subbase materials and also meeting with the specification of JTG/E51-2009(21) was directly used. All the gradations were showed in Table 1.

TABLE 1 The gradations of base and subbase materials

Size(mm) / Category	Passing (%)							
	31.5	26.5	19	9.5	4.75	2.36	0.6	0.075
100% WTA for sub-base	99	96.9	89.7	74.7	55.1	37.6	19.3	9.5
Subbase upper limits	100	100	100	100	100	100	30	0
lower limits	50	50	50	50	50	17	17	0
NO.1 (virgin aggregates)	91.6	59.4	15.7	5.2	1.1	0.5	0.5	0.1
NO.2 (virgin aggregates)	100	100	66.4	33.6	6.3	0.2	0.2	0.1
Combined blend for base	97.7	89.7	72.6	52	38.7	26.4	13.6	6.7
Base upper limits	100	94	83	64	50	36	19	7
lower limits	90	81	67	45	30	19	0	0

Specific gravity and Water Absorption

The WTA was divided into coarse aggregate CA (retained on 2.36mm sieve) and fine aggregate FA (passing 2.36mm sieve). The values of both apparent specific gravity and bulk specific gravity and water absorption of the WTA and virgin aggregates obtained from the tests were summarized in Table 2.

TABLE 2 Specific gravity and water absorption of WTA and virgin aggregates

Aggregate category	Apparent specific gravity	Bulk specific gravity	Water absorption (%)
CA of WTA	2.63	2.08	10.17
FA of WTA	2.54	1.91	11.58
NO.1 (virgin aggregates)	2.73	2.70	0.46
NO.2 (virgin aggregates)	2.73	2.68	0.59

Mechanical Properties:

WTA: The crushing strength value (an index of aggregate resistance to crushing) and LA Abrasion value of WTA were 25.8% and 37.7%, respectively. Both of them met the specifications of JTG/T F20-2015(22).

VIRGIN AGGREGATE: The crushing value and LA Abrasion values were 14% and 14.8%, both of them met the specifications of JTG/T F20-2015.

(IJRST) 2018, Vol. No. 8, Issue No. II, Apr-Jun **e-ISSN: 2249-0604, p-ISSN: 2454-180X**

Cement

Composite Portland cement was, coded P.C.32.5 by Chinese classification, used in this study, i.e., the compressive strength of (Cement mortar strength) is 32.5 MPa. It was a commercial available and provided by HaiLuo Pavement Construction Co. Ltd, Suzhou, China.

Proctor compaction test

The maximum dry density and the optimum moisture content (OMC) were determined by proctor compaction test. Standard heavy-duty compaction specified by Chinese code was used in this study, i.e., a 4.5kg hammer with a drop height of 450mm compacted 98 blows for each of the three layers. The weight of the sample was 5100g. The proctor compaction results were listed in Table 3. The OMCs were used to make samples for all the performance tests in this study.

TABLE 3 OMC and maximum dry density

Cement content (%)		3	4	5
OMC (%)	Base	9.4	9.5	9.7
	Subbase	11.6	11.8	12.1
Maximum dry density (g/cm^3)	Base	2.026	2.034	2.047
	Subbase	1.905	1.921	1.929

TEST METHODS

X-ray Diffraction (XRD)

The X-ray diffraction spectrum is obtained by the specific diffraction direction and intensity of the solid crystalline powder to the X-ray. The test device can effectively identify and analyze common phases. The test specimen size of RTA was 100 mm × 100 mm × 400 mm in the middle beam, cured for 7 days in an environment chamber with a temperature of 20 °C and humidity over 95% before the test. The specimen was ground into powder of less than 0.075 mm. The curing condition for the samples were selected the same as that for strength tests to understand the formation mechanism of the strengths.

Scanning Electron Microscope (SEM)

SEM is used to acquire various physical and chemical properties of the test samples of RTA, such as morphology, composition, crystal structure, electronic structure and internal electric or magnetic field and the like.RTA samples were ground into powders with a particle size of less than 0.075mm.

(IJRST) 2018, Vol. No. 8, Issue No. II, Apr-Jun **e-ISSN: 2249-0604, p-ISSN: 2454-180X**

Unconfined compression and splitting tensile strength

The cylinder specimens with size of Φ150mm × 150mm were cured for 7 days in a curing box of constant temperature of 20 ℃ and humidity of 95% before testing according to specifications (JTG/E51-2009).The loading rate for both the splitting and unconfined compression tests was at 1mm/min.The maximum pressure P was recorded and the unconfined compressive strength was calculated according to formula (1)

$$R_c = \frac{P}{A} \quad (1)$$

In the formula: R_c– specimen unconfined compressive strength (MPa)

P – Maximum pressure load (N)

A – Specimen cross-sectional area (mm^2)

In the split test, a bar was placed on the press table of the press. Place the specimen horizontally on the bar and place a layer on the top surface of the specimen. The maximum pressure P was recorded, and the splitting strength of the specimen was calculated according to formula (2)

$$R_i = 0.004178\frac{P}{h} \quad (2)$$

In the formula: R_i– The splitting strength (MPa)

P – Test the maximum force value when the failure (N)

h – Specimen height (mm)

Dry shrinkage

The test specimen size was a beam of 100 mm × 100 mm × 400 mm and cured for 7 days in the same environment as used for the unconfined compression specimens. The dry box temperature was set at20 °C and the humidity was set to 60%. To allow the specimen to move freely by shrinking, the specimens were placed on glass bars. The deformation was measured by a dial indicator, following the specifications (JTG/E51-2009)

Take the readings on the four dial indicators on the sample at the i^{-th}step , X_{i1}, X_{i2}, X_{i3} and X_{i4}. Weigh the weight of each specimen mi. The specimens were dried to a constant weight of m_p.

The rate of water loss was calculated according to formula (3)

$$W_i = (m_i - m_{i+1})/m_p \quad (3)$$

Where: W_i – The i^{-th} water loss rate (%)

m_i– The i^{-th} weighing weight of specimen (g)

m_p – Specimen weight at dry condition (g)

(IJRST) 2018, Vol. No. 8, Issue No. II, Apr-Jun **e-ISSN: 2249-0604, p-ISSN: 2454-180X**

The dry shrinkage according to the formula (4) calculation

$$\delta_i = (\sum_{j=1}^{4} X_{i,j} - \sum_{j=1}^{4} X_{i+1,j})/2 \quad (4)$$

Where: δ_i– The i-th dry shrinkage observed (μm)

$X_{i,j}$ – Reading of the j-th dial gauge for the i-th test (μm)

Calculation of dry shrinkage strain according to formula (5)

$$\varepsilon_i = \delta_i / l \quad (5)$$

Where:ε_i – the dry shrinkage strain of i (%)

δ_i– the dry shrinkage measured by i (μm)

l– the length of the standard specimen (mm)

Temperature shrinkage

The size, curing time and conditions of the specimens were the same as those for the dry shrinkage test**.** After curing, the samples were placed in the oven of 105 ℃ and dried for 10~12 hours until the weight was constant, which the thermal shrinkage measured can exclude the moisture effect. The temperature range chosen for the test was 40 ℃ ~ -10 ℃. Starting with the up limit of 40 ℃, the temperature was then reduced by an interval of 10 ℃ for every three hours.The calculation formula (4) and (5) were used for temperature shrinkage also.

Frost Resistance

The size and curing conditions of the specimens for frost were the same as those of unconfined compressive strength specimens, except that a curing date of 28 days was used.Nine specimens were used for 5 freeze-thaw cycles, nine specimens for no freeze-thaw. Each cycle specimens need to be frozen for 18 hours at a temperature of -18 ℃, and then be placed in 20 ℃ of water for 8 hours.The weight of the specimen after each freeze-thaw cycle was measured during the test. After 5 freeze-thaw cycles, the samples were tested for compressive strength R_{DC}. Frost resistance performance according to formula (6) (7)

$$\text{BDR} = \frac{R_{DC}}{R_C} \times 100 \quad (6)$$

Where: BDR – Loss of compressive strength after n cycles of freeze-thaw (%)

R_{DC}– Compressive Strength after n cycles of freeze-thaw of the specimen (MPa)

R_C – The compressive strength of test pieces for control (no freeze-thaw) (MPa)

$$W_n = \frac{m_0 - m_n}{m_0} \times 100 \quad (7)$$

Where: W_n – Weight change rate of specimen after n cycle of freeze-thaw (%)

m_0– Weight of the specimen before freeze-thaw cycle (g)

m_n– Specimen weight after n cycle of freeze-thaw (g)

Fatigue Performance

The size and curing conditions of the specimens for fatigue performance were the same as those for dry shrinkage, except that a curing duration of 90 days was adopted. MTS810 test machine, see Figure 2, was selected for the study. The type of loading is sine wave with the frequency of 10Hz. Preload pressure of 20% of the maximum flexural tensile strength was applied for 2 minutes.The number of parallel test groups was 5, and the final fatigue life value was taken as an arithmetic mean of the five samples.

Figure 2The fatigue test

RESULTS AND DISCUSSIONS

MICROSCOPIC ANALYSIS

Prior to the test, samples with a particle size larger than 4.75mm and between 0.075~4.75mm were ground into powders for microscopic examination. Presented in the section included those of WAT sieved in three different size and one without sieving. The differences in sharp and chemical element were discussed.

Figure 3 was the original WTA (without sieving) taken from SEM.

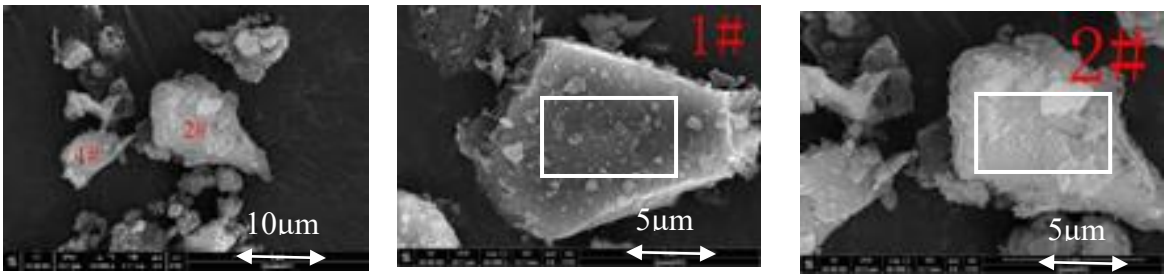

(IJRST) 2018, Vol. No. 8, Issue No. II, Apr-Jun **e-ISSN: 2249-0604, p-ISSN: 2454-180X**

a) WTA（in5μm） b) Point 1（in5μm） c) Point 2（in4μm）

d) Elemental composition of Point 1 e)Elemental composition of Point 2

FIGURE 3 The SEM results of original WTA (without sieving)

In general, as showed in Figures 3 a), the WTA particles were mostly crystals in an irregular shape, most importantly, some crystals were covered with a layer of gel. Two randomly-selected points 1 and 2 on the crystals were presented on Figures 3, b) and c), in a

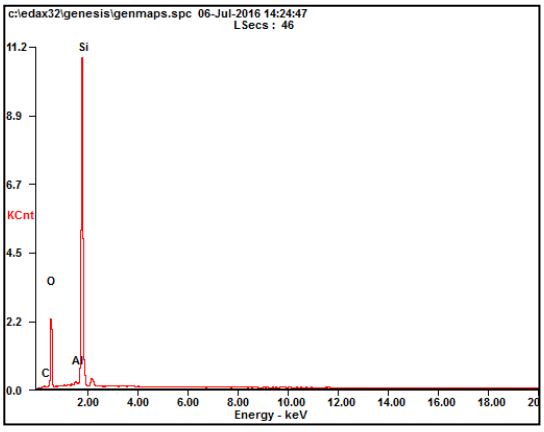

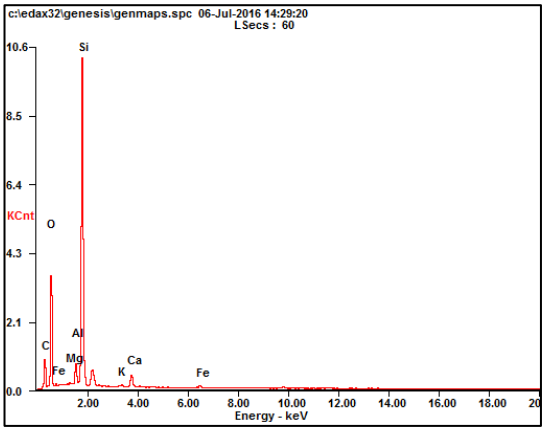

large scale, indicating clearer edges and angles, and flatter surfaces for point 1 than point 2. Point 2 particle, however, attached with a thicker layer of gel obviously than that attached on Point 1.

Elements of Si and O as the main elements for the crystals that might be mainly from quartz. Point 2 contained more elements of Mg, K, Ca, Fe and other elements than Point 1, see Figures 3, d) and e). The difference in the elements between the two points of 1 and 2 could result from that in the thickness of the surface gels, mostly from hydrated calcium silicate gel. In addition, an H element was not found in the elemental analysis spectrum, indicating that hydrated calcium silicate was highly carbonized(23).

Figures 4 were the SEM results taken from coarse WTA (>4.75mm). As can be seen from the Figure 4 a), clouds of crushed particles and crystal particles were presented closely. The small particles have no flat surfaces and angles. The big particles have clear surfaces. Figures 4, b) and c) were, again for a close look at the Points 3 and 4 selected from Figure a). Point 3 particle has a clear outline, and has a more regular shape than Point 4 which was regarded as the crushed gel. Figures 4, d) and e), indicated that the main chemical elements were Si, O, Al for both the points discussed.There were no big differences in the types of elements, but there were differences in density observed.Point 3 had much more elements of Ca and C than Point 4 because it contained more calcium carbonate.

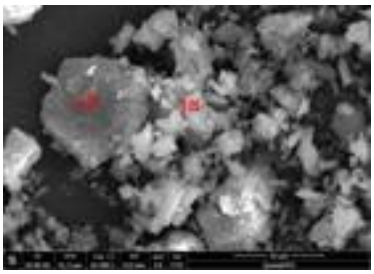

a) WTA (in 10μm)

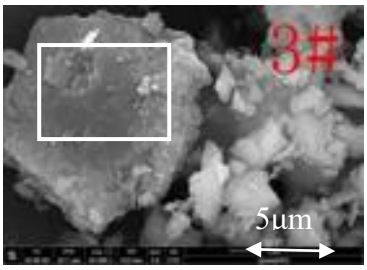

b) Point 3 (in 5μm)

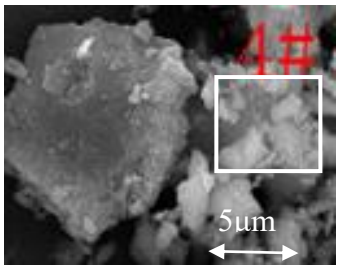

c) Point 4 (in 5μm)

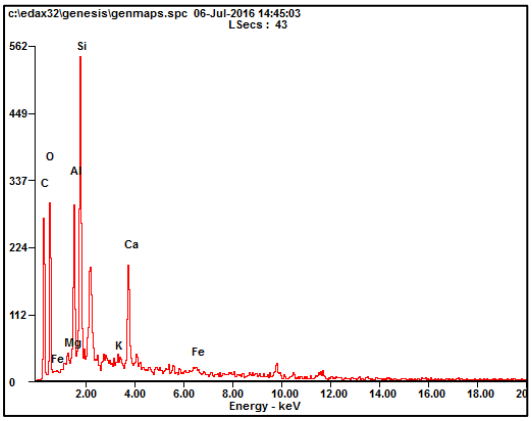

d)Elemental composition of point 3

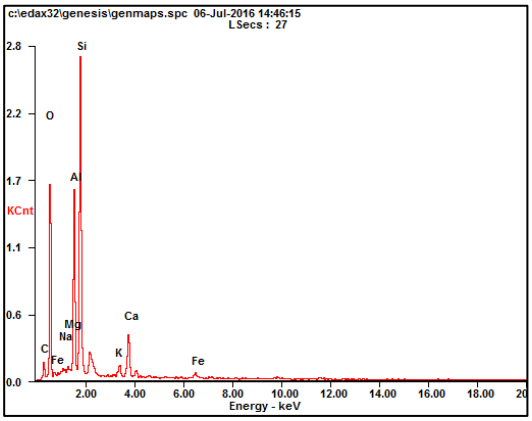

e)Elemental composition of point 4

FIGURE 4 The SEM results of coarse WTA (>4.75mm)

Figures 5 were the SEM results for middle WTA (0.075 mm ~ 4.75 mm). As can be seen from the Figure 5 a), the crystals were completely cemented to form a gel structure, appeared on aggregates as a denser layer. The particles were highly carbonated calcium silicate hydrated material as compared to coarse WTA (> 4.75mm). This showed that calcium silicate hydration was much more completed. Figures 5 c) and d) were SEM taken for a close look at the Points 5 and 6, indicating that Points 5 and 6 were gel and all with rough surfaces. Figures 5 e) and f) showed that elements of Points 5 and 6 were no difference. The content of Si in Point 5 was remarkably higher than that in Point 6. But the contents of Al, O and Fe in Point 5 were lower than those in Point 6. This was mainly due to the fact that Point 6 contained more fly ash. Also, compared with Figures, there were many other elements that comes from fly ash.

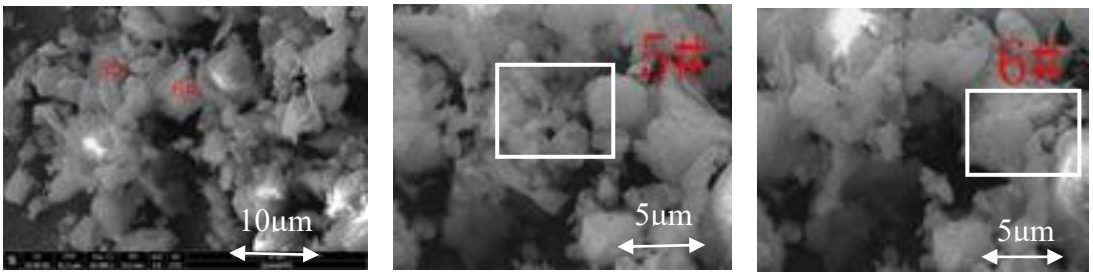

a) WTA (in 10µm) b) Point 5 (in 5µm) c) Point 6 (in 5µm)

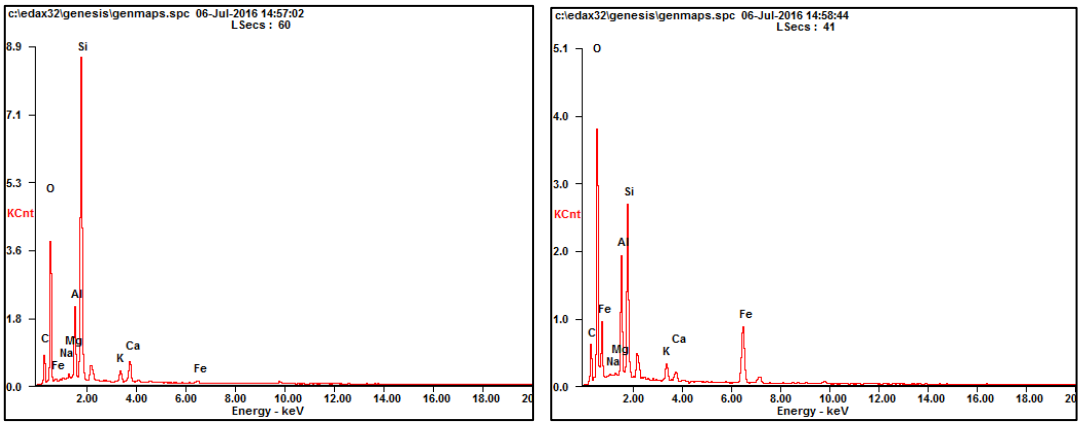

d)Elemental composition of point 5 e)Elemental composition of point 6

FIGURE 5 The SEM results of middle WTA (0.075mm ~ 4.75mm)

Figures 6 were SEM results from fine WTA (< 0.075 mm). It can be seen from the Figure 6 a), the shape of the WTA was not the kind of polygonal edges with rough corners, but more like a ball shape. The substances with corner polygons were predominantly silicon oxide. The spherical shapes observed in the Figure conform to those of fly ash, inferring that the ball like particles were fly ash left from hydration.Further, compared with WTA (0.075 mm~4.75 mm), the WTA(< 0.075 mm) has gels mainly attached to a single particle rather than cemented with the various particles, and has much more content of gel. Figures 6 b) and c) showed Point 7 particle was irregular shape, clustered together into irregular "cloud" materials. Point 8 particle surface was relatively smoother, separately dispersed. As can be seen from the Figures 6 d) and e), there was no obvious difference in elements found between Points 7 and 8, but Point 7 contained more Al and O than Point 8. This showed that Point 7 contained more alumina than Point 8.

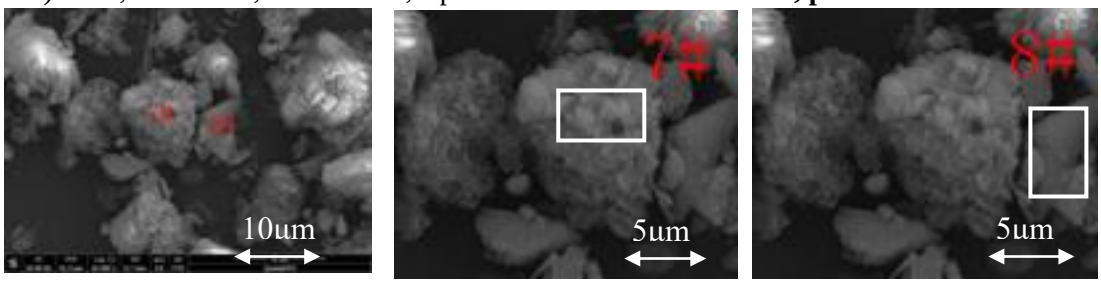

a) WTA (in 10μm) b) Point 7 (in 5μm) c) Point 8(in 5μm)

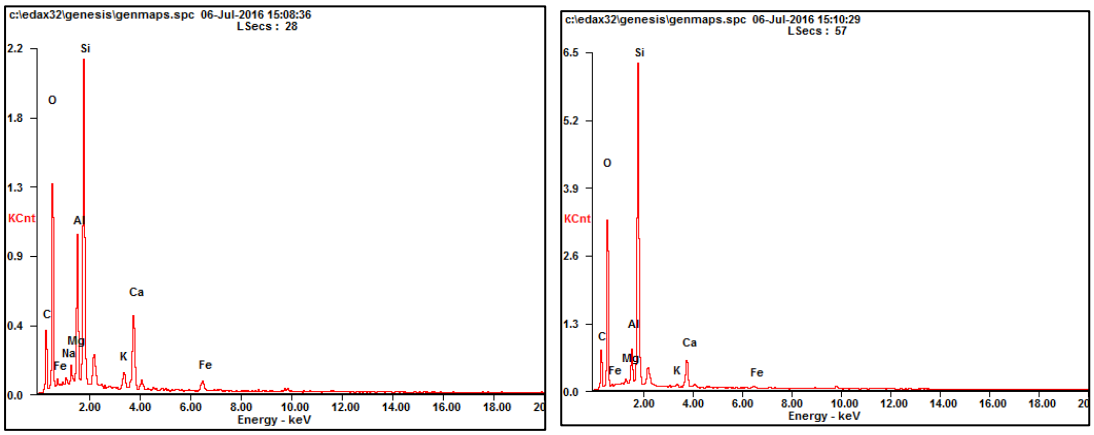

d)Elemental composition of Point 7 e)Elemental composition of Point 8

FIGURE 6 The SEM results of fine WTA (<0.075mm)

As conclusions,WTA was mainly composed of irregular crystals and irregular gels regardless of the size. The crystals were mainly quartz, and the gels mainly highly carbonated calcium silicate hydrate, though, the compositions of WTA were somewhat sizes-dependent. Fine WTA (<0.075 mm) also contained fly ash. Middle WTA (0.075 mm ~ 4.75 mm) contained the most gel, and the coarse WTA (>4.75 mm) the least gel. Besides, the roughness of the particles increased as the particle size decreased.

STRENGTH CHARACTERISTICS

The unconfined compressive strength and splitting indirect tensile strength of Portland cement stabilized RTAs cured for 7 days were presented in Figure 7.

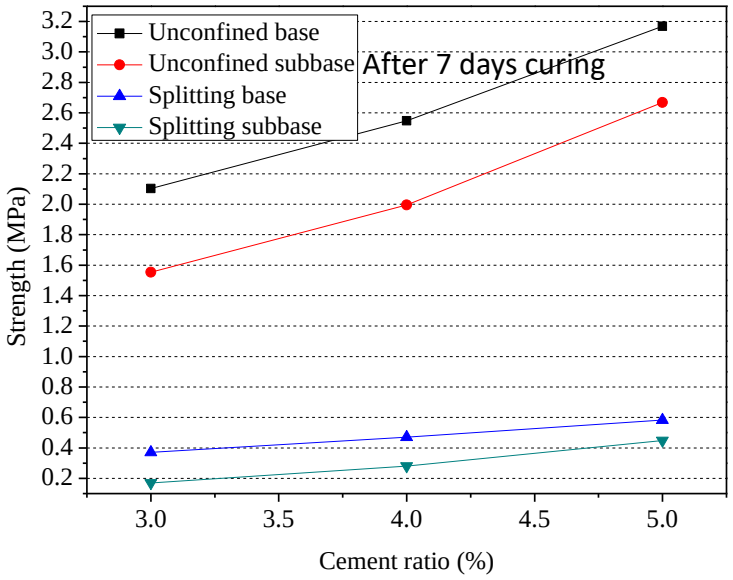

FIGURE 7 The unconfined compressive and splitting indirect tensile strength (After 7 days curing)

It can be seen from Figure 7 that the unconfined compressive strength, splitting indirect tensile strength of base layer were larger than those of the subbase layer as expected. This was partially because the base largely used some new aggregates and a better gradation. As the cement content increased, the unconfined compressive strength and splitting direct tensile strength of the RTA obviously increased at a similar rate, again, as expected.

In order to analyze the mechanism of the strength change with the cement content, XRD test was carried out on the subbase layer with different cement used. The experimental XRD patterns were summarized in Figure 8 and the height of the peaks associated with the intensity in the graph was summarized in Table 4.

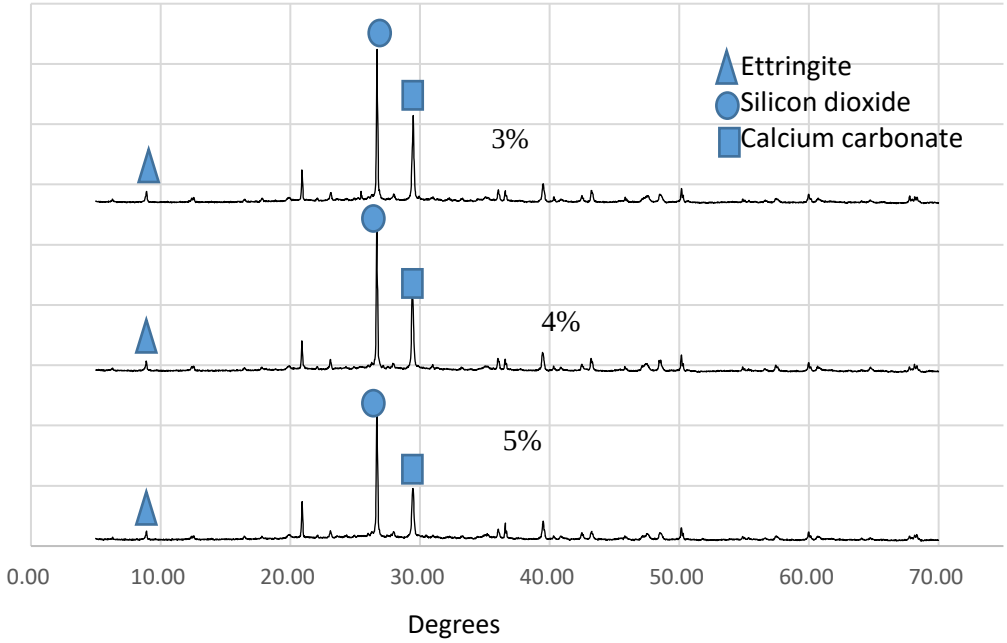

FIGURE 8The XRD patterns of subbase layer with different cement contents

TABLE 4 The height of the peaks

Substance type		Cement content (%)		
		3	4	5
Height	Ettringite	470	560	566
	Quartz	10010	11304	11101
	Calcium carbonate	3246	5032	4600

Ettringite improves the early strength of concrete or cementitious materials, or produces shrinkage compensation for concrete, while the delayed ettringite formation causes concrete cracking damage (24, 25). The height of ettringite peak increased and the strength of specimen increased accordingly with the increase of cement content, see Table 4. Height of calcium carbonate and silica also played a positive role in strength, as in general. The contents of both calcium carbonate and silica increased as the cement content increased.

Accordance to JTG/T F20-2015, the 7th day unconfined compressive strength of cement stabilized base material should be greater than 2 MPa, and that of the subbase layer should be greater than 1 MPa. The unconfined compressive strength of base and subbase with 3% cement content was slightly higher than the specification requirements. For the sake of engineering economy, this study selected 4% cement content.

DRY SHRINKAGE

The relationship between the measuring time and the water loss was shown in Figure 9.

(IJRST) 2018, Vol. No. 8, Issue No. II, Apr-Jun **e-ISSN: 2249-0604, p-ISSN: 2454-180X**

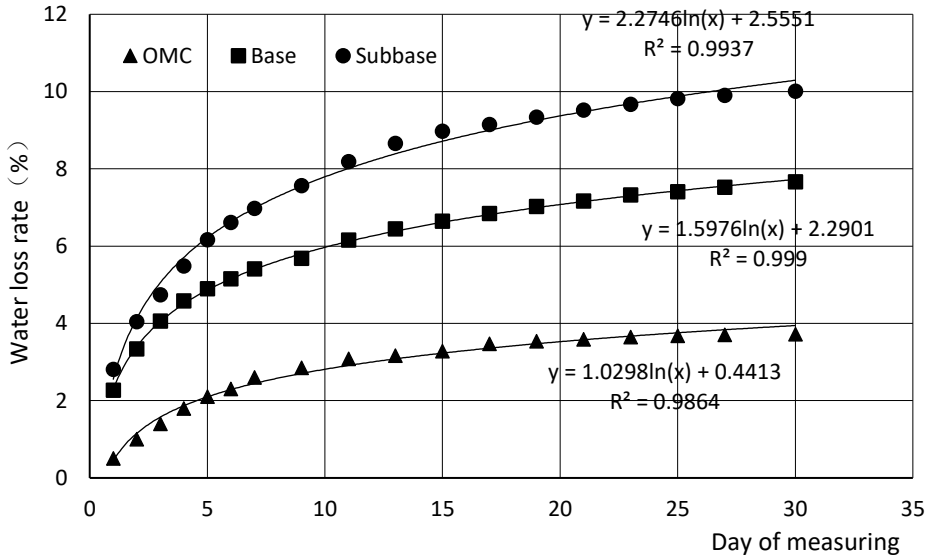

FIGURE 9 The relationship between the measuring time and the water loss

From figure 9, the water loss was increased with the increase of the days for OMC and base /subbase RTAs, while the water loss of the RTAs were higher than that of OMC, mainly because RTAs contained WTA, and the water absorption of WTA was higher than that of virgin aggregate. In addition, both the RTAs and OMC had a quicker water loss rate in early period of bout10 days than later.

Detailed analysis on the water loss was made in the following. On the 30th day, the water loss rate of the subbase RTA was 10%, the water loss rate of base RTA was 7.7%, and the water loss rate of OMC was 3.7%, accounting for about 86%, 83% and 95% of the water absorption, respectively. On the 7th day, the water loss of the base / subbase RTAs and OMC were 5.4%, 7% and 2.3% accounting for 57.5, 57.7% and 62.2% of the water absorption, respectively. The findings indicated that the water losses were closely correlated with the water contents absorbed, and was very fast in the early stage.

Empirical regressions between the water loss and the measuring time were made for base / subbase RTAs and OMC. The water loss and the curing time were in logarithmic relation with high R^2, see Figure 9. By regression formula, the number of days needed for RTAs and OMC to complete dry was 54 for subbase RTA, 85 for base RTA and 35 for OMC.Again, it indicated that the water loss will take 2-3 months for RTAs and 1-2 months for OMC, but the first 7 days will lose about 60% of all the water loss.

Similarly, regressions between the day of measuring and the shrinkage were shown in Figure 10.

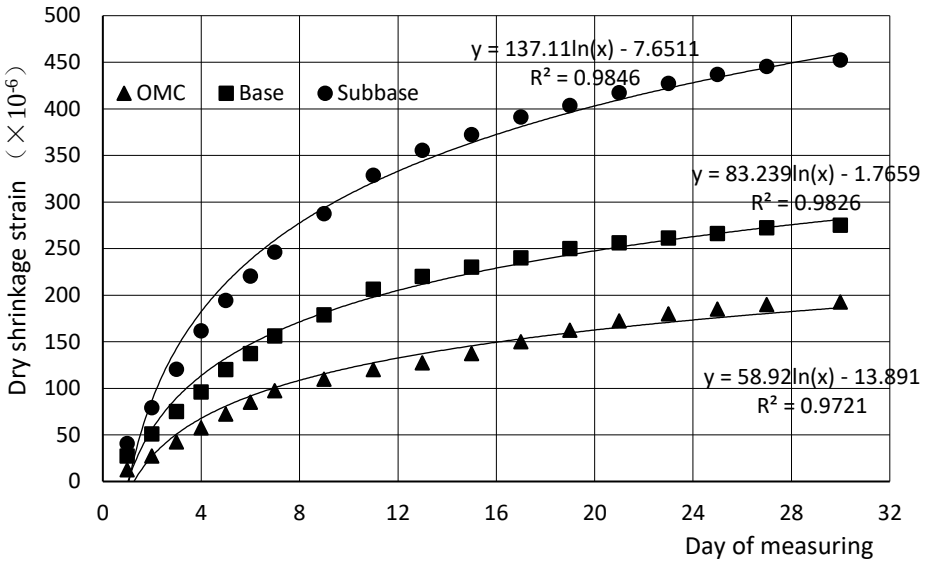

FIGURE 10 The relationship between the time and the shrinkage

The total dry shrinkage strain of the base / subbase RTAs and OMC in 30 days were 275×10^{-6} ,452×10^{-6} and 192×10^{-6}, while in 7th day were 156×10^{-6} and 246×10^{-6} and 97.5×10^{-6} respectively. The ratio of the 7 days shrinkage accounted for 57%, 54% and 50% of those of 30 days for the base / subbase RTAs and OMC, respectively, see Figure 10. The results showed that the dry shrinkage performance of subbase RTA was larger than the base RTA, and the dry shrinkage performance of RTAs were larger than OMC.The fast shrinkage speed was attributed from the water loss in the earlystage, i.e., original from the high percentage of WTA used for base / subbase RTAs.

The equationobtained by regression showed that the shrinkage and the curing time were in logarithmic relation. The shrinkage limits of the base / subbase RTAs and OMC were 367×10^{-6}, 539×10^{-6}, and 195×10^{-6}estimated by using the days at which the water loss was complete.

The relationship between water loss and dry shrinkage was shown in Figure 11.

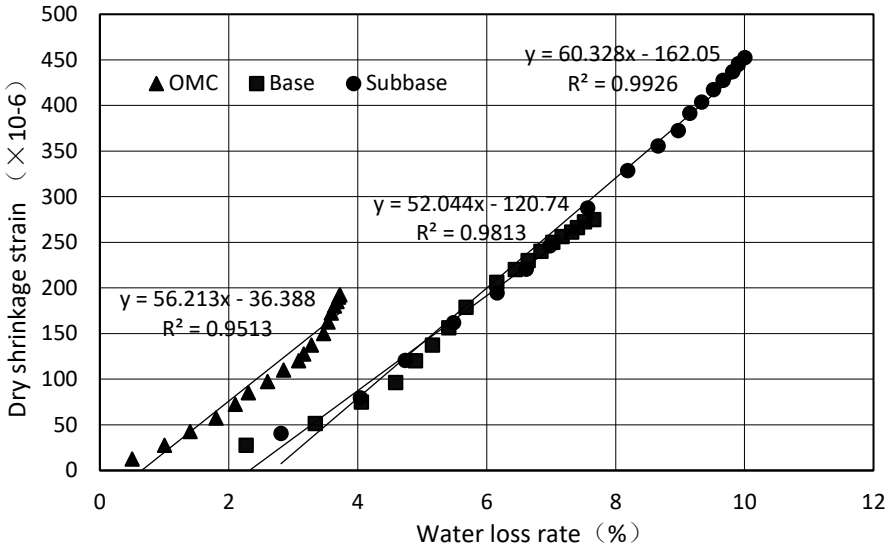

FIGURE 11 The relationship between water loss and dry shrinkage strain

Figure 11 indicated that the relationship of dry shrinkage strain with the water loss was very close for both base RTA and subbase RTA, which were a liner line with high values of R^2. Again, the results indicated the nature of the dry shrinkage strain, i.e., the loss of water contents added in the RTA. Using the OMCs the RTAs were made with,the base and subbase RTAs shrinkage strain limit were calculated to be $365\times10^{-6}$and 657×10^{-6}, respectively.

Subbase RTA's water loss was higher than that of base RTA's, and base RTA's water loss was higher than that of OMC's, the dry shrinkage strain also shows the same rule, which was mainly due to the water absorption of WTA higher than that of virgin aggregate. The surface of RTA (<4.75mm) was relatively smooth, see SEM pictures, the other RTA surface were rougher. These rough surfaces greatly increased the difficulty of RTA for compaction.The coarser the particle surfaces, the greater the dry shrinkage strain.

TEMPERATURE SHRINKAGE

The cement-stabilized RTA temperature shrinkages were summarized in Table 5.

TABLE 5 Results of temperature shrinkage strain

Temperature (°C)		40to 30	30 to 20	20 to 10	10 to 0	0 to -10
Base RTA	Net	95	88	81	74	66
$\times10^{-6}$	Total	95	184	265	338	404
Subbase RTA	Net	103	98	92	88	84
$\times10^{-6}$	Total	103	201	294	381	466

It can be seen from Table 5 that the total temperature shrinkage increased as temperature decreased. The total temperature shrinkage strain were 466×10^{-6}, and 404×10^{-6} for subbase and

(IJRST) 2018, Vol. No. 8, Issue No. II, Apr-Jun **e-ISSN: 2249-0604, p-ISSN: 2454-180X**

base RTAs, respectively.As the temperature decreased, the temperature shrinkage strain decreased in each temperature range. When the temperature of the base layer was reduced from 40 ℃ to 20 ℃ (taking into account the actual probability of occurrence of the higher and most unfavorable), the amount of shrinkage of 201×10^{-6} and 6 days before the sample shrinkage strain corresponding to the base layer was 184×10^{-6} equivalent to the specimen 10 days before the amount of shrinkage strain, which showed that the change of temperature was also a key factor leading to the occurrence of cracks.

FROST RESISTENCE

The average change in the weight of the RTA blends was shown in Figure 12.

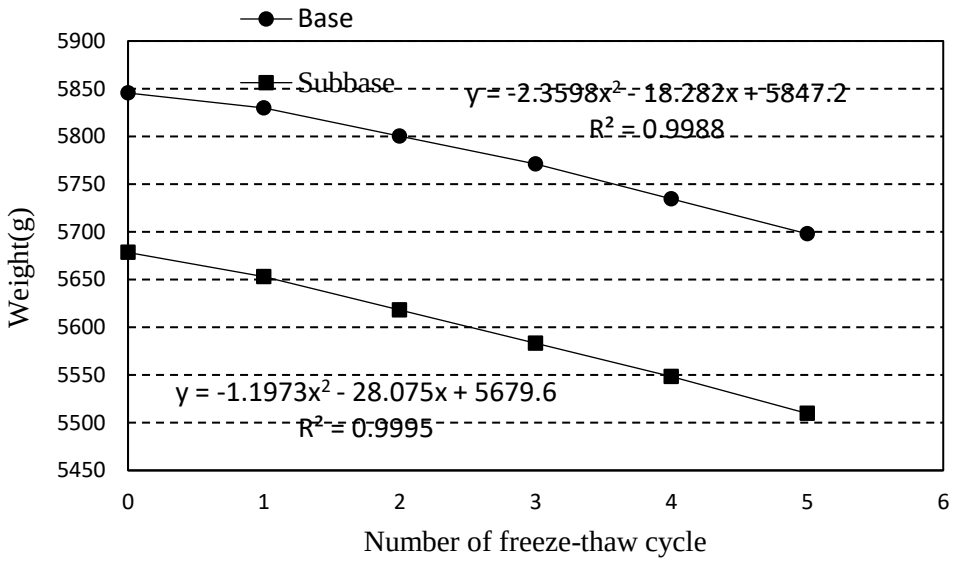

FIGURE 12 Freeze-thaw cycles and the weight of the test pieces

It can be seen from Figure 12 that the mass change rate W_n after 5 times of the freeze-thaw cycle were 2.97% and 2.52% for base and subbase RTAs respectively. The required W_n was 5% higher than base and subbase, so that the unconfined compressive strength test can be carried out.

The strengths of the specimen after n freeze-thaw cycles (R_{DC}) were 2.624 MPa and 2.289 MPa, and the strength of specimen before freeze-thaw (R_C) were 3.716 MPa and 2.589 MPa, for base and subbase RTAs, respectively. Generally, the weight loss of the two RTAs did not show big difference even the subbase RTA contained a high WTA than the base RTA.

The compressive strength loss (BDR) of the base RTA was 70.6% and that of the subbase RTAs was 88.4%.Existing studies have shown that in severe frozen areas, the BDR of 28 day's semi rigid base after 5 freeze-thaw cycles should be greater than 50%. In this study, both the base and subbase RTAs' BDR were greater than 50%, so the cement stabilized RTAs have a

good frost resistance.

FATIGUE PERFORMANCE

The ratios of the loading stress to the flexural-tensile strength used in this study were 0.55 and 0.7. The specimen was placed and loaded on the mold with the four-point pressure method. The fatigue test results were summarized in Table 6.

Table 6 Summary of fatigue test results

Type of specimen	Flexural-tensile strength (MPa)	Stress Ratio	Fatigue life (cycles)
Base RTA	0.456	0.55	401174
		0.7	8109
Subbase RTA	0.312	0.55	104757
		0.7	3249

It can be seen from the Table 6 that the fatigue performance of the base RTA was better than that of the subbase RTA under the two stress ratios as expected. The RTA with a high WTA would decrease a lot of the fatigue life. When the stress ratio increased from 0.55 to 0.7, the life of both the base and subbase RTA decreased sharply at a similar decreasing rate of about 97%. Studies have shown that the fatigue life of semi-rigid base was different in different gradation types. Among them, the skeleton compact type has the longest fatigue life, the suspended dense type is the shortest, and the skeleton void type is slightly worse than the skeleton dense type. The fatigue life of cement stabilized RTA was closer to that of suspension dense type (the fatigue life was 200 thousands ~ 600 thousands cycles in the 0.55 stress ratio and 2 thousand ~7 thousand cycles in the 0.7 stress ratio).

SUMMARY AND CONCLUSIONS

This study investigated the feasibility of using recycled Lime-flyash stabilized aggregated (RTA) as either base or subbase layer of a pavement. Long-term properties of Portland cement stabilized RTA were examined in terms of shrinkage, freeze-thaw, fatigue properties. Based on the test results, following conclusions can be drawn:

1) As the particle size decreases, the roughness of the RTA particles increases. The roughness of particles was closely related to OMC obtained from the compaction and to the dry shrinkage strain. The coarser the particles, the greater the dry shrinkage strain.

2) The total dry shrinkage strain was increased as the water loss increased. The water content was in logarithmic relationship with the curing time, which was a similar way between to the shrinkage and the curing time.

3) The RTA blends exhibited a linear relationship between the temperature shrinkage and temperature decrease at each interval. So the maximum temperature should be avoided to

(IJRST) 2018, Vol. No. 8, Issue No. II, Apr-Jun **e-ISSN: 2249-0604, p-ISSN: 2454-180X**

reduce the formation of temperature cracks in hot weather.

4) The fatigue performance of the base RTA was better than that of the subbase RTA under all the two stress ratios used in the study.

REFERENCES

1. XU Yue-zhou, SHI Jian-guang, Analyses and evaluation of the behavior of recycled aggregate and recycled concrete, Concrete, No. 201 Number 7 in 2006. (in Chinese)
2. Juan Li,Influence of Mortar Adhesive to Recycled Aggregates on Strength of Concrete and Research of Lime-fly Ash Stabilized Recycled Aggregate, Master Thesis, Ho Hai University, 2005. (in Chinese)
3. Nataatmadja, A. & Tan, Y. Resilient response of recycled concrete road aggregates. Journal of Transportation Engineering, 127, 450-453, 2001.
4. Bestgen, Janile O., Hatipoglu, Mustafa, Cetin, Bora, Mechanical and Environmental Suitability of Recycled Concrete Aggregate as a Highway Base Material, Journal of Materials in Civil Engineering, Vol. 28, No.9, 2016, pp. 1535-1543.
5. Hotineanu, Anca; Bouasker, Marwen; Aldaood, Abdulrahman, Effect of freeze-thaw cycling on the mechanical properties of lime-stabilized expansive clays, Cold Regions Science and Technology, Vol 116–117, pp281–288, 2015.
6. Xue, Y., Hou, H., Zhu, S., Zha, J., Utilization of municipal solid waste incineration ash in stone mastic asphalt mixture: pavement performance and environmental impact. Constr. Build. Mater. 23, 989–996, 2009.
7. Goswami, R. K., and Mahanta, C. “Leaching characteristics of residual lateritic soils stabilised with fly ash and lime for geotechnical applications.” Waste Manage. 27(4), 466–481, 2007. (in Chinese)
8. TENG Xu-qiu, CHEN Zhong-da, JIANG Wan-min, Journal of Chang'an University (Natural Science Edition), Vol.26 No.1, Jan. 2006.
9. SUN Yong-hong , SHA Ai-min, Influence of Coarse Aggregate Skeleton on Road Performance of Lime-fly-ash Stabilized Crushed Stone, Journal of Highway and Transportation Research and Development, Vol. 30 No. 6 Jun. 2013.
10. Khogali, W. E., and Mohamed, E. H. H. “Novel approach for characterization of unbound materials.” Transportation Research Records 1874, Transportation Research Board, Washington, DC, 2004.
11. Lekarp, F., Isaccson, U., and Dawson, A. “State of the art: I: Resilient response of unbound aggregates.” J. Transp. Eng., 10.1061 / (ASCE) 0733-947X126:1(66), 66–75, 2000.
12. Yuan, D., Hoyos, L. R., and Puppala, A. J. “Evaluation and mix design of cement-treated base materials with high RAP content.” 90thAnnual Meeting of the Transportation Research Board, Washington, DC, 2011.

13. MDSHA (Maryland State Highway Administration). "Maryland roadway design manual." <http://www.roads.maryland.gov/m/index.aspx?PageId=453> Nov. 20, 2015.
14. Cetin, B., Aydilek, A. H., and Li, L. "Experimental and numerical analysis of metal leaching from fly ash-amended highway bases." Waste Manage, 32(5), 965–978, 2012b.
15. Komonweeraket, K., Cetin, B., Aydilek, A. H., Benson, C. H., and Edil, T. B. "Effects of pH on the leaching mechanisms of elements from fly ash mixed soils." Fuel, 140, 788–802, 2015.
16. Berthelot, C., Podborochynski, D., Marjerison, B., and Gerbrandt, R. (2009). "Saskatchewan field case study of triaxial frequency sweep characterization to predict failure of a granular base across increasing fines content and traffic speed applications." J. Transp. Eng., 10.1061/ (ASCE) TE.1943-5436.0000054, 907–914.
17. Thom, N. H., and Brown, S. F. "Effect of moisture on the structural performance of a crushed-limestone road base." Transportation Research Records 1121, Transportation Research Board, Washington, DC, 1987.
18. WANG Yan , NI Fu-jian , LI Zai-xin, Test Research on Influential Factor for Shrinkage Performance of Cement-treated Macadam Base, Journal of Highway and Transportation Research and Development, Vol.24 No.10, Oct. 2007. (in Chinese)
19. Khogali, W. E., and Mohamed, E. H. H. "Novel approach for characterization of unbound materials." Transportation Research Records 1874, Transportation Research Board, Washington, DC, 2004.
20. Dempsey, B. J. "Core flow-capacity requirements of geocomposite fin-drain materials used in pavement subdrainage." Transportation Research Records 1159, Transportation Research Board, Washington, DC, 1988.
21. JTG/E51-2009, Test methods of materials stabilized with inorganic binders for highway engineering, [S].
22. JTG/T F20-2015, Technical guidelines for construction of highway roadbases, [S].
23. Feng Xiaoxin, Zheng Wei. SEM study of high alkali silicate cement clinker [J]. Cement Engineering, 2013, (05): 21-23. [2017-09-16]. DOI: 10.13697 / j .cnki.32-1449 / tu.2013.05.012
24. Yang Jiansen. Ettringite duality of the role of the concrete conditions of its occurrence [J] Civil Engineering Journal, 2003, (02): 100-103 [2017-09-16] DOI.10.15951 / j. tmgcxb .2003.02.020
25. ZHANG Zhao-peng, CHU Zhong-xin, LI Ying-kun. Peak height and peak area statistics indicate differences in the relative content of clay minerals core [J]. Ocean Science, 2016, 40 (12): 107-113. [2017-09-16].